Radiation and Environmental Biophysics
https://doi.org/10.1007/s00411-017-0729-y

ORIGINAL ARTICLE

In vitro studies of DNA damage and repair mechanisms induced by BNCT in a poorly differentiated thyroid carcinoma cell line

C. Rodriguez[1] · M. Carpano[1] · P. Curotto[3] · S. Thorp[2] · M. Casal[4] · G. Juvenal[1,5] · M. Pisarev[1,5] · M. A. Dagrosa[1,5]

Received: 10 February 2017 / Accepted: 24 December 2017

Abstract

Boron neutron capture therapy (BNCT) for aggressive tumors is based on nuclear reaction [^{10}B (n, α) ^{7}Li]. Previously, we demonstrated that BNCT could be applied for the treatment of undifferentiated thyroid carcinoma. The aim of the present study was to describe the DNA damage pattern and the repair pathways that are activated by BNCT in thyroid cells. We analyzed γH2AX foci and the expression of Ku70, Rad51 and Rad54, main effector enzymes of non-homologous end joining (NHEJ) and homologous recombination repair (HRR) pathways, respectively, in thyroid follicular carcinoma cells. The studied groups were: (1) C [no irradiation], (2) gamma [^{60}Co source], (3) N [neutron beam alone], (4) BNCT [neutron beam plus 10 µg ^{10}B/ml of boronphenylalanine (^{10}BPA)]. The total absorbed dose was always 3 Gy. The results showed that the number of nuclear γH2AX foci was higher in the gamma group than in the N and BNCT groups (30 min–24 h) ($p < 0.001$). However, the focus size was significantly larger in BNCT compared to other groups ($p < 0.01$). The analysis of repair enzymes showed a significant increase in Rad51 and Rad54 mRNA at 4 and 6 h, respectively; in both N and BNCT groups and the expression of Ku70 did not show significant differences between groups. These findings are consistent with an activation of HRR mechanism in thyroid cells. A melanoma cell line showed different DNA damage pattern and activation of both repair pathways. These results will allow us to evaluate different blocking points, to potentiate the damage induced by BNCT.

Keywords Damage · Repair · Pathways · BNCT · Thyroid cancer

Introduction

Boron neutron capture therapy (BNCT) is a binary radiation treatment. It consists of the administration of a non-toxic compound containing stable ^{10}B atoms that are selectively incorporated into tumor cells. The ^{10}B atom irradiated with thermal neutrons turns into ^{11}B, an unstable isotope that instantaneously undergoes nuclear fission, releasing an alpha particle and a lithium nucleus [^{10}B(n, α)^{7}Li]. These heavy particles are both of high linear energy transfer (LET), they have short, energetic tracks and deposit most of their energy within the boron-containing cells. Thus, the tumor cells are selectively killed without causing severe damage to the normal tissue (Coderre and Morris 1999). BNCT is particularly well suited to treat aggressive cancers that do not respond to conventional treatments such as malignant gliomas, melanomas and recurrent head and neck cancers (Joensuu et al. 2011). Clinical trials are being carried out in several countries around the world such as Italy, Finland, Taiwan, Japan and Argentina (Aiyama et al. 2011; Busse et al. 2003; Aihara et al. 2006).

Some years ago, we demonstrated in our laboratory that BNCT could be applied for the treatment of undifferentiated and poorly differentiated thyroid carcinoma (Dagrosa et al. 2002, 2003, 2007), which lost their capability to accumulate iodine. Therefore, the usually applied therapeutic dose

✉ M. A. Dagrosa
dagrosa@cnea.gov.ar

1 Radiobiology Department (CAC, CNEA), 1499 Gral Paz Av, Buenos Aires, Argentina

2 Instrumentation and Control Department (CAE, CNEA), 15 Presbítero González y Aragón Rd, Buenos Aires, Argentina

3 RA-3-Investigation and Production Reactors (CAE, CNEA), 15 Presbítero González y Aragón Rd, Buenos Aires, Argentina

4 Oncology Institute "Ángel H. Roffo"-University of Buenos Aires, 5481 San Martín Av, Ciudad Autónoma de Buenos Aires, Argentina

5 Scientific and Technical Research National Council (CONICET), 1917 Rivadavia St, Ciudad Autónoma de Buenos Aires, Argentina

Published online: 16 February 2018

of radioactive iodine is ineffective. These tumors are very aggressive and have a fatal outcome within a short time after the diagnosis (Pasieka 2003).

DNA damage and repair mechanisms activated by BNCT have been poorly studied. Ionizing radiation produces a wide spectrum of DNA lesions, such as base damage, sugar damage, single strand breaks (SSB), double strand break (DSB), and DNA–DNA and DNA–protein cross links. The spectrum of induced lesions and their distribution are affected by the radiation quality (Maier et al. 2016; Belli et al. 2002). Among these kinds of lesions, the DSB seems to be the most important in producing biological effects. It is widely accepted that unrepaired or misrepaired DSBs lead to the formation of chromosome aberrations, cell killing and transformation (Wang et al. 2010). In previous studies, we showed that BNCT produces larger and more complex chromosome aberrations (micronuclei) than conventional radiotherapy in tumor cells (Dagrosa et al. 2011a, b).

One of the earliest steps after induction of a DSB is the phosphorylation of the histone H2AX (γH2AX) (Burma et al. 2001). This histone is phosphorylated at serine 139 by the ATM kinase. Once DNA repair is finished, γH2AX is dephosphorylated and, therefore, γH2AX focus formation, quantity and size are used as a DSB marker (Redon et al. 2010).

DSBs induced in the DNA of higher eukaryotes (Olive 1998) by ionizing radiation are repaired either by non-homologous end joining (NHEJ) or by homologous recombination repair (HRR) mechanisms (Lieber 2010; Sigurdsson et al. 2002). NHEJ acts through DNA-PK, Ku70, Ku80 and DNA ligase 4 enzymes and HRR acts through the products of Rad52 epistasis gene family (Rad51, Rad52, Rad54, Rad55, Rad57 and Rad58). Which DSB repair pathway is triggered in each situation remains unknown, but it could depend on the inducing agent and the cell cycle phase in which cells are arrested (Pawlik et al. 2004; Vermeulen et al. 2008). HRR is typically associated with DNA replication when homologous DNA on a sister chromatid or chromosome acts as template to guide the broken strand repair (Dudas et al. 2004). On the other hand, NHEJ is a less accurate form of DSB repair, in which the two DNA broken edges are processed to form compatible ends that are directly ligated (Weterings and Chen 2008). The evaluation of relative contribution of NHEJ and HRR to ionizing radiation-induced DNA DSB repair is important for the understanding of the mechanisms leading to tumor cell death by BNCT.

The aim of this study was to analyze the DNA damage pattern and the repair pathways that are activated by BNCT in poorly differentiated thyroid carcinoma cells. To achieve this goal, we evaluated γH2AX foci frequencies and their size. Moreover, we evaluated the expression of Ku70, Rad51 and Rad54 which are the main effector enzymes of the NHEJ and HRR pathways. We performed the same measurements using gamma radiation and a melanoma human cell line to compare the results with another type of carcinoma.

Materials and methods

Cell lines

The human thyroid follicular cancer cell line, WRO (kindly provided by Dr. Julliard, UCLA, USA), was grown in RPMI-1640 medium (GIBCO, Invitrogen Corporation, USA) supplemented with 154 mg/mL sodium pyruvate, 1.5 g/L sodium bicarbonate, 10 mg/mL streptomycin, 1,000,000 UI/L penicillin and 10% foetal bovine serum (FBS, Natocor, Córdoba, Argentina).

The human melanoma cell line, Mel J (provided by Dr. Mordoh, Leloir Biochemistry Investigation Institute, Argentina), was grown in high-glucose DMEM medium (GIBCO, Invitrogen Corporation, USA) supplemented with 3.7 g/L sodium bicarbonate, 10 mg/mL streptomycin, 1,000,000 UI/L penicillin, 2 mM glutamine and 10% fetal bovine serum (FBS, Natocor, Córdoba, Argentina).

Both cell lines were maintained at 37 °C in a 5% CO_2 and 95% humidified atmosphere.

Boron solution

The stock solution of boronphenylalanine (^{10}BPA) was prepared in a concentration of 30 mg ^{10}BPA per mL (0.14 M). The BPA (95% enriched in ^{10}B atoms L-phenylalanine isomer, Boron Biologicals Inc., Raleigh, USA) was combined in water with fructose in a 1:1 ratio and the pH was adjusted to 9.5–10 with 10 N NaOH with constant stirring until complete dissolution. The final pH was 7.4 and was adjusted carefully with 6N HCl. The solution was sterilized with a 0.22 μm syringe filter.

Dosimetry

Gamma irradiations were carried out in a ^{60}Co source (1 Gy/min) in the ^{60}Co chamber of the Oncology Institute "Angel H. Roffo". Neutron irradiations were carried out at the RA-3 reactor thermal column facility (Miller et al. 2009) at Ezeiza Atomic Centre (CAE), Buenos Aires, Argentina, where a highly thermalized and homogenous irradiation field is available. Thermal neutron flux was 5.9×10^{11} n/cm^{2}min^{-1}; the cadmium ratio was 4100 for gold foils, which allowed neglecting the fast neutron dose. The gamma dose rate was approximately 6.0 ± 0.2 Gy/h. In both cases, different time lapses were selected to achieve a total physical dose of 3 Gy (± 10%) (Tables 1, 2, 3, 4).

The thermal neutron flux was determined using a self-powered detector based on rhodium, which was calibrated

Table 1 Dosimetry for thermal neutron irradiation (N) without boron

Irradiation time (min)	Thermal neutron flux (n/cm^2 min^{-1})	Fluence (n/cm^2)	Dose γ (Gy)	Dose ^{14}N (Gy)	Total dose (Gy)
9.88	$5.9\times10^{11}\pm5\times10^{10}$	$5.78\times10^{12}\pm5\times10^{11}$	1.385 ± 0.043	1.61 ± 0.14	3.0 ± 0.1

Table 2 Dosimetry for thermal neutron irradiation (N plus 10 ppm ^{10}B)

Irradiation time (min)	Thermal neutron flux (n/cm^2 min^{-1})	Fluence (n/cm^2)	Dose γ (Gy)	Dose ^{14}N (Gy)	Dose ^{10}B (Gy)	Total dose (Gy)
3.7	$5.9\times10^{11}\pm5\times10^{10}$	$2.16\times10^{12}\pm2\times10^{12}$	0.519 ± 0.017	0.604 ± 0.051	1.87 ± 0.16	3.0 ± 0.2

Table 3 Average foci number per nucleus after irradiation with gamma rays and a neutron beam (gamma, N and BNCT)

Time	C	Gamma	N	BNCT
30 min	12 ± 5	28 ± 7 *	20 ± 9	24 ± 7
1 h	11 ± 4	27 ± 6	19 ± 7	18 ± 6
2 h	15 ± 6	24 ± 8	22 ± 7	18 ± 5
4 h	14 ± 6	19 ± 7	20 ± 7	18 ± 6
24 h	10 ± 4	13 ± 4	9 ± 5	13 ± 6

Table 4 Average foci size (μm^2) per nucleus after irradiation with gamma rays and a neutron beam (gamma, N and BNCT)

Time	C	Gamma	N	BNCT
30 min	0.28 ± 0.08	0.8 ± 0.16	0.6 ± 0.16	0.9 ± 0.18*
1 h	0.35 ± 0.12	0.7 ± 0.07	0.7 ± 0.17	0.9 ± 0.27
2 h	0.3 ± 0.09	0.75 ± 0.07	0.7 ± 0.23	0.78 ± 0.22
4 h	0.3 ± 0.05	0.7 ± 0.21	0.55 ± 0.18	0.73 ± 0.26
24 h	0.53 ± 0.26	0.8 ± 0.21	0.6 ± 0.18	0.73 ± 0.15

using cobalt chips. The epithermal and fast neutron flux determinations were performed with low cadmium activation flakes and indium low cadmium flakes and a boron sphere, respectively. The results of these measurements were several orders of magnitude lower than those obtained for the heat flux; so, they were not taken into account for dose calculation. Finally, for the neutron beam dose calculation, a graphite ionization chamber reinforced with a lithium cap was used.

Experimental design

The treatment groups were: (1) C (no irradiation), (2) gamma (irradiation with the ^{60}Co source), (3) N (irradiation with a neutron beam alone), (4) BNCT (irradiation with a neutron beam plus ^{10}BPA).

The day prior to the irradiation, cells in exponential growth phase (between 50 and 70% confluent) were seeded in T25 or p60 dishes according to the experiment. ^{10}BPA (10 μg ^{10}B/ml, 0.925 mM final) was added to cell culture medium (BNCT group) 12–16 h before irradiation, the time at which there is a maximum in^{10}BPA uptake in thyroid tumor cells (Dagrosa et al. 2011a, b).

Immunofluorescence

At different times after the irradiation (30 min, 1, 2, 4 and 24 h), the cells were fixed in paraformaldehyde 4% in PBS 1× for 15 min, then they were permeabilized with 0.5% Triton X-100 in PBS 1× for 15 min at 4◦C and blocked with 5% fetal bovine serum also diluted in PBS 1× (Ibañez et al. 2009). Next, the cells were incubated overnight with a monoclonal anti-γH2AX antibody (Upstate, Lake Placid, NY) in a 1:500 dilution in water. Next day, the cells were incubated with a secondary antibody anti-mouse IgG (Upstate, Lake Placid, NY) coupled to FITC in a 1:200 dilution in water for 1 h. Finally, each sample was mounted in Vectashield with DAPI antifade solution.

Images were obtained with a CCD camera (Olympus DP70) coupled to an Olympus BX51 fluorescence microscope with a 100× lens (UPlanApo 100/1.35 oil). About 100 cells per sample in triplicate were analyzed for determining the average number of foci per nucleus and more than 100 cells to determine the average focus size per nucleus. To measure both parameters, Image Pro Plus and Origin Pro 8 software were used.

RT-PCR

2, 4, 6, 24 and 48 h after irradiation, total RNA was extracted using TRIzol reagent isolation protocol (Invitrogen Life Technologies). RNA quantification was performed in a Nano Drop 2000 (Thermo Scientific) with 1 μL of the RNA extraction product. Reverse transcription was carried out with 2 μg of total RNA with SuperScript III™ Reverse Transcriptase protocol (Invitrogen Life Technologies) using Oligo $(dT)_{12-18}$ primers (Biodynamics). PCR was performed in a thermocycler (Mrc, Scientific Instruments) using Promega

Master Mix standard protocol that consisted of 30 cycles at 95 °C for 45 s, specific temperature according to each primers for 45 s and 72 °C for 45 s. Primer sequences used were: Rad51 (59 °C), PF: 5′-CTTTGGCCCCACAACCCATTTC-3′, PR: 5′-ATGGCCTTTCTCACCTCCAC3′ (Jen-Chung Ko et al. 2008), Ku70 (56 °C), PF: 5′-CATGGCAACTCCAGAGCAG-3′, PR: 5′-GCTCCTTAAACTCATCCACC-3′ (Korabiowska et al. 2004), Rad54 (53 °C), PF: 5′-AAGTGTGTGGAAGAGGAG-3′, PR: 5′-CCAATGAGATTGAGGCCA-3′ (Matsuda et al. 1999). The PCR products were visualized in a 2% agarose gel with GelRed Nucleic Acid Stain (Biotium). The images obtained in an EC3 Imaging System were analyzed with the program Image J and the intensity of each band was related to a standard gene, in this case GADPH.

Protein expression assay

For *Western blot* analysis, cells were incubated at 37 °C during 2, 4, 6, 24 and 48 h after irradiation. Cells were washed twice in cold PBS, scrapped and centrifuged. The pellet was lysed in 100µL RIPA buffer (1 M Tris–HCl, pH 7.2, 1 M NaCl, 1% Nonidex P-40, 0,5% sodium deoxycholate, 0.1% SDS) containing proteases inhibitors. The protein concentration was determined by Bradford protein assay (BioRad). From each sample, 40 µg of total protein was loaded in a 10% SDS-acrylamide:bisacrylamide gel and electrophoresis was carried out first at 170 V and then at 200 V (~ 27 V/cm). Proteins were transferred to a *Hybond-P* membrane (Amersham) in transfer buffer (25 mM Tris-base, 192 mM glycine, 20% methanol, 0.05% SDS) at 100 V for 1 h at 4 °C. Membranes were incubated in blocking solution, 5% bovine serum albumin (BSA) in phosphate buffer with Tween-20 0.05% (PBS-T), and probed with rabbit antibodies raised against Rad51 (Santa Cruz Biotechnology) and Ku70 (Calbiochem) overnight in a 1:200 dilution in BSA. Beta-actin monoclonal antibody (Clone AC-15, Sigma) was used as a loading control. Membranes were washed and incubated for 1 h with the secondary antibody anti-rabbit IgG horseradish peroxidase conjugated (Calbiochem) in a 1:5000 dilution in BSA. The bands were visualized by chemiluminescence after the addition of substrate (ECL detection kit, Amersham) and exposed to autoradiography films (Amersham Hyperfim™ ECL). Semiquantitative analysis was performed by measuring each band density. The relative optical density (OD) was obtained by dividing the density of each band by the beta-actin density.

Statistical analysis

All results are expressed as the average of three independent experiments ± SEM. For statistical analysis of foci number and size, Tukey–Kramer multiple comparison test was performed, and for gene and protein expression differences, Student–Newman–Keuls multiple test was used.

Results

Nuclear γH2AX foci were stained to evaluate the formation and repair of DSBs in WRO cells. Figure 1 shows representative images of cells irradiated with 3 Gy of radiation arising from the different treatments (gamma, N and BNCT). The quantification of foci per nucleus (Fig. 2) demonstrated that the focus number was higher in cells irradiated with gamma rays (γ) than in cells irradiated with neutrons N ($p < 0.001$) and BNCT ($p < 0.001$) at all the times of evaluation. The difference between BNCT and N groups was also significant ($p < 0.001$) at all the times except at 4 h. From 4 to 24 h after the irradiation, focus numbers tended to decrease. This observation is expected due to DNA repair. However, the analysis of focus size showed that foci are larger in cells treated by BNCT as compared to those in the N and gamma groups. The difference is significant ($p < 0.01$) from 30 min post-irradiation (Fig. 3). At 24 h, the focus size did not decrease significantly in any group.

Expression of HRR repair enzymes Rad51 and Rad54 showed a radiation-induced increase. After 4 h post-irradiation, Rad51 mRNA expression increased significantly ($p < 0.05$) in cells irradiated with neutrons with or without previous incubation with BPA as compared to those treated by gamma irradiation and control cells (Fig. 4). Twenty-four hours post-irradiation, decreased Rad51 mRNA levels were observed. At 48 h, these levels were stabilized. Rad54 mRNA levels increased 6 h after the irradiation in N and BNCT groups and were stabilized at 48 h as Rad51 (Fig. 5). The expression of Ku70, a member of the NHEJ pathway, did not show significant differences in mRNA levels, neither between groups nor at any fixation time (Fig. 6). [For further understanding, Rad51 and Ku70 Western Blot protein expression assays were made (Fig. 7)].

The analysis of proteins showed that Rad51 protein levels increased 4 h after irradiation (Fig. 8) and remained elevated for 48 h in the BNCT group. In contrast, Ku70 protein levels did not show significant changes, although demonstrated a tendency to decrease compared to control cells (Fig. 9). These findings are consistent with an activation of HRR mechanism in WRO cells irradiated with neutrons alone or with boron compound (N and BNCT).

To find out if DNA damage and repair mechanisms induced by BNCT were specific to the follicular thyroid carcinoma cell line (WRO), the same parameters were evaluated in a human melanoma cell line (Mel J). Foci number increased in BNCT and N groups compared to control group (C) 30 min after irradiation (the number was higher in N than in the BNCT group), but after 24 h

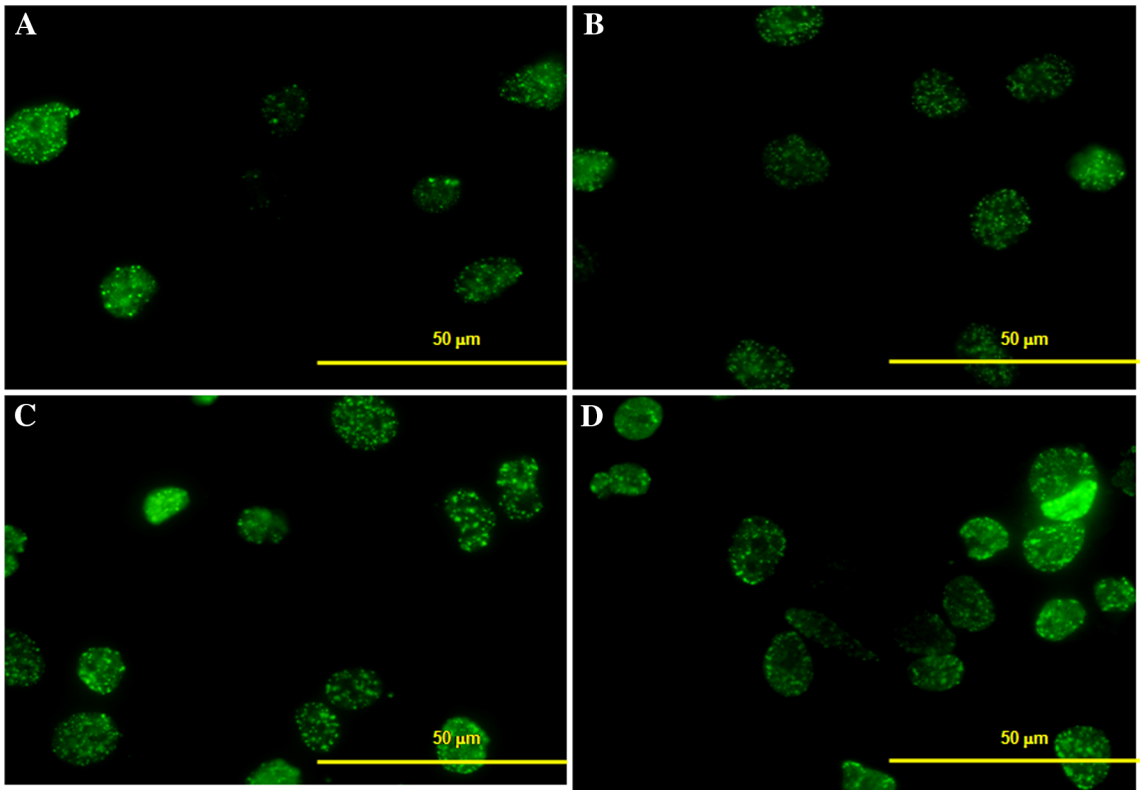

Fig. 1 Representative images of γH2AX foci in control WRO cells (**a**), those irradiated with gamma rays (**b**) and with a neutron beam in the absence (N) or presence of BPA (BNCT) after 30 min, images **c** and **d**, respectively

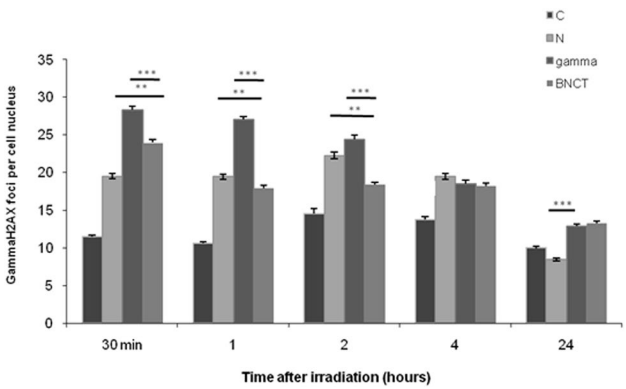

Fig. 2 γH2AX focus numbers per nucleus as function of time after irradiation (30 min, 1, 2, 4 and 24 h) in WRO non-irradiated cells (C), cells irradiated with gamma rays, cells without BPA irradiated with a neutron beam (N) and cells with BPA irradiated with a neutron beam (BNCT). C vs N, gamma, BNCT ***$p < 0.001$; BNCT vs N **$p < 0.01$; BNCT vs gamma ***$p < 0.001$

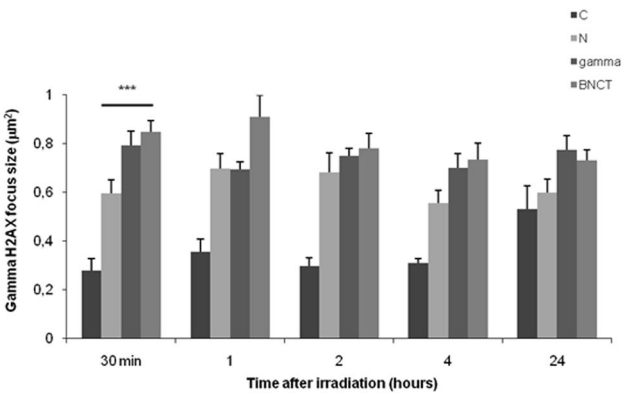

Fig. 3 γH2AX focus size per nucleus as function of time after irradiation (30 min, 1, 2, 4 and 24 h) in WRO non-irradiated cells (C), cells irradiated with gamma rays, cells without BPA, irradiated with a neutron beam (N), and cells with BPA, irradiated with a neutron beam (BNCT). BNCT vs N **$p < 0.01$

this number seemed to decrease (Fig. 10). The mean focus size was higher in cells treated by BNCT compared to the N group ($p < 0.001$) 30 min after irradiation, reaching the basal levels 24 h post-irradiation in both groups (Fig. 11). These results could suggest that in this melanoma cell line, DSBs are more scattered, better distributed along the DNA molecule but not clustered (non-DSB clustered lesions), resulting in a more efficient DNA repair process. On the other hand, the study of the repair genes expression showed an increase of Rad51 mRNA 2 h after the irradiation (Fig. 12) and an increase also in Ku70 mRNA at 4 h post-irradiation. In contrast to WRO cells, both repair

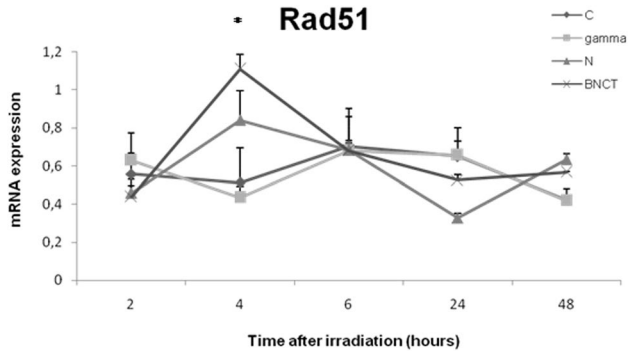

Fig. 4 Rad51 mRNA expression as function of time after irradiation (2, 4, 6, 24 and 48 h) in non-irradiated WRO cells (C), cells irradiated with gamma rays, cells without BPA irradiated with a neutron beam (N), and cells with BPA, irradiated with a neutron beam (BNCT). Gamma vs BNCT $*p < 0.05$

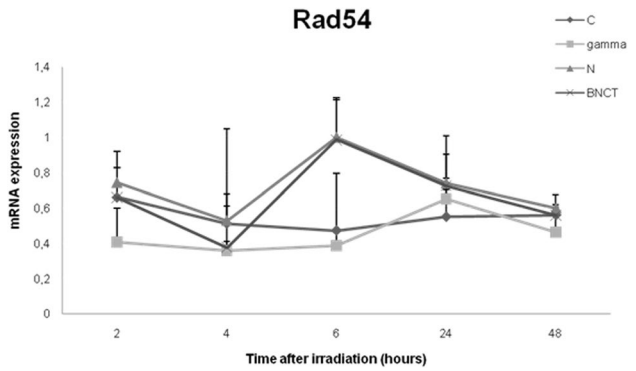

Fig. 5 Rad54 mRNA expression as function of time after irradiation (2, 4, 6, 24 and 48 h) in non-irradiated WRO cells (C), cells irradiated with gamma rays, cells without BPA, irradiated with a neutron beam (N), and cells with BPA, irradiated with a neutron beam (BNCT)

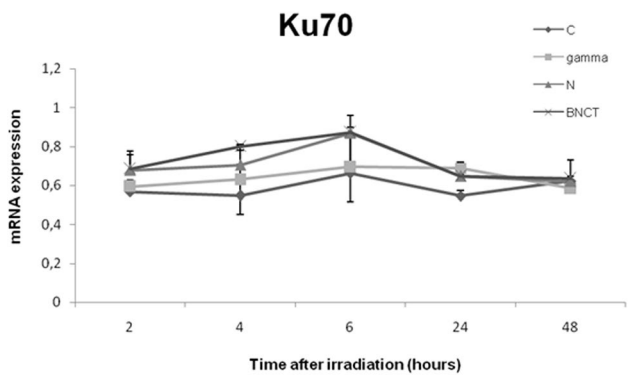

Fig. 6 Ku70 mRNA expression as function of time after irradiation (2, 4, 6, 24 and 48 h) in non-irradiated WRO cells (C), cells irradiated with gamma rays, cells without BPA, irradiated with a neutron beam (N), and cells with BPA, irradiated with a neutron beam (BNCT)

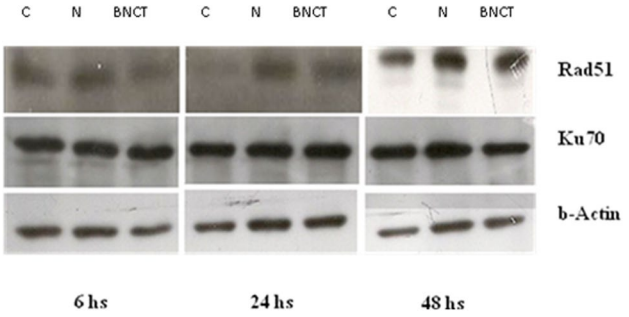

Fig. 7 Analysis of Rad51 and Ku70 by Western Blot. WRO cells irradiated with a neutron beam in the absence (N) or presence of BPA (BNCT) after 6, 24 and 48 h and in cells control no irradiated (C)

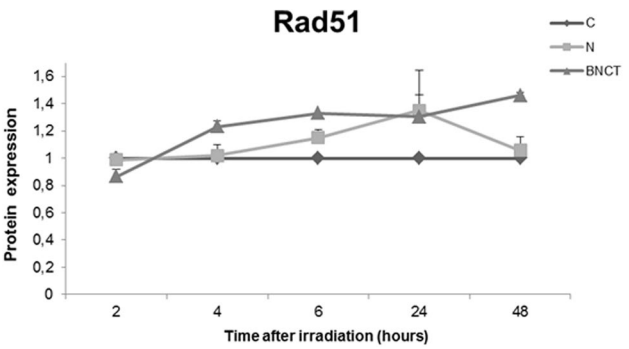

Fig. 8 Rad51 protein expression as function of time after irradiation (2, 4, 6, 24 and 48 h) in WRO non-irradiated cells (C), cells without BPA, irradiated with a neutron beam (N), and cells with BPA, irradiated with a neutron beam (BNCT)

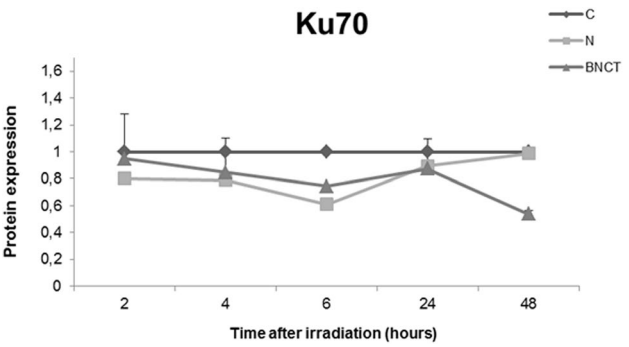

Fig. 9 Ku70 protein expression as function of time after irradiation (2, 4, 6, 24 and 48 h) in WRO non-irradiated cells (C), cells without BPA, irradiated with a neutron beam (N), and cells with BPA, irradiated with a neutron beam (BNCT)

pathways (HRR and NHEJ) could be activated by BNCT in Mel J (Fig. 13).

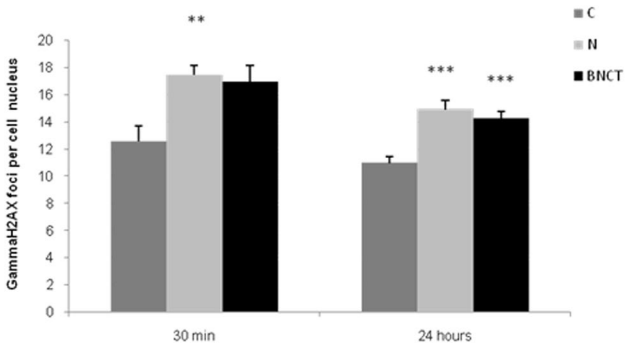

Fig. 10 γH2AX focus numbers in Mel J cells after 3 Gy of irradiation with a neutron beam with or without BPA (N and BNCT). Results are expressed as average number of foci per nucleus, per treatment and per time

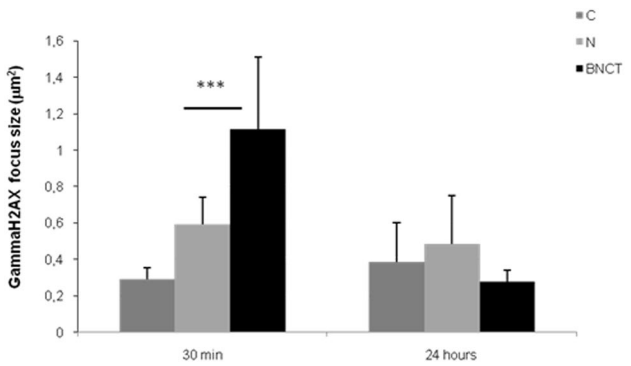

Fig. 11 γH2AX focus size in Mel J cells after 3 Gy of irradiation with a neutron beam with or without BPA (N and BNCT). Results are expressed as average foci size per nucleus, per treatment and per time. N vs BNCT 30 min ***$p < 0.001$

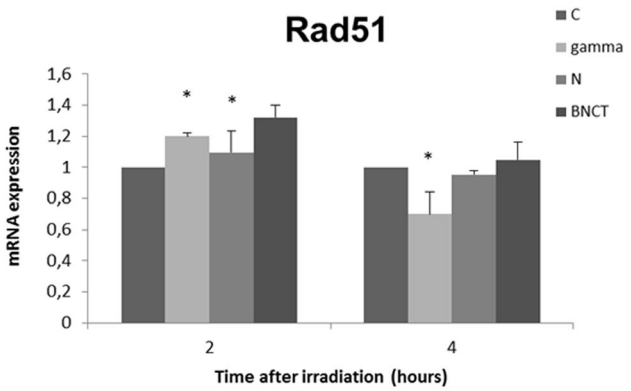

Fig. 12 Rad51 mRNA expression as function of time after irradiation in non-irradiated Mel J cells (C), cells irradiated with gamma rays, cells irradiated with a neutron beam (N) and cells with BPA, irradiated with a neutron beam (BNCT)

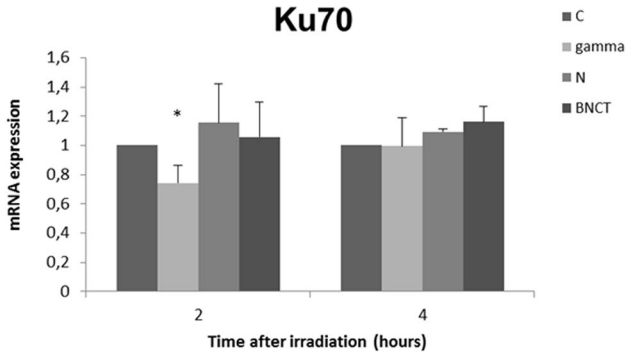

Fig. 13 Ku70 mRNA expression as function of time after irradiation in non-irradiated Mel J cells (C), cells irradiated with gamma rays, cells irradiated with a neutron beam (N) and cells with BPA irradiated with a neutron beam (BNCT)

Discussion

The application of BNCT to clinical treatments of some types of cancers has committed several multidisciplinary groups to work on two fundamental aspects of this binary system: the development of new boron-10 compounds and their administration, and tumor irradiation with more accurate and effective neutron beams (Coderre and Morris 1999). Previously, we demonstrated that BNCT could be applied for the treatment of undifferentiated and poorly differentiated thyroid carcinoma (Dagrosa et al. 2002, 2003, 2007). In this work, we studied the DNA damage and the repair mechanisms induced by irradiation arising from BNCT in a human follicular thyroid carcinoma cell line. The results were compared to a reference melanoma cell line.

Little has been investigated about the underlying DNA damage response mechanisms activated by BNCT. The knowledge of these radiobiological mechanisms would allow to manipulate the tumor response to radiation and thus achieve a therapeutic improvement. Particularly, we focused on the DNA as BNCT target since it constitutes one of the most sensitive molecules within the cell. The severity of the induced lesions and their spatial distribution depend on the radiation quality. It is expected that densely ionizing radiation produces clustered ionizations with relatively high efficiency (Wang et al. 2010).

Unlike conventional radiotherapy modalities based on low LET radiation, the radiation field during BNCT consists of a mixture of components with different LET characteristics. The total absorbed physical dose results from the sum of those individual physical doses. In addition to the dose from capture reaction in boron-10, the neutron beam interacts with different elements in the tumor, resulting in a background mixture of high and low LET radiation. Within the nonspecific dose components, the neutron capture reaction by hydrogen atoms releases a 2.23 MeV gamma ray,

while thermal neutrons captured in nitrogen releases a high LET proton with an average energy of 590 keV. Also, the fast neutrons which contaminate the neutron beam produce recoil protons of high LET [^{1}H (n, n′) p] by collisions with hydrogen nuclei, with average energies similar to protons from nitrogen. Gamma rays are induced from the reaction of neutron capture in H [^{1}H (n, gamma) ^{2}H], but also from the contributions of the beam and the activation of the material shielding and collimated beam that is around the patient support. Therefore, studying the radiobiological effects arising from BNCT consists in evaluating the effects of a complex radiation beam with many dose components.

In this paper, we evaluated DNA damage through the detection of H2AX histone phosphorylation foci. γH2AX has been measured by other groups after irradiation with low or high LET radiation (Burma et al. 2001; Ibañez et al. 2009).We observed that focus numbers during the evaluated time were lower for N and BNCT groups than for the gamma group. In all studied groups, the highest focus numbers were found 30 min after irradiation. The group irradiated with gammas showed the highest number of foci. The low foci number in cells irradiated with neutrons was also seen in cells irradiated with another type of particles (Antonelli et al. 2015). However, when we measured the focus size, we observed that it was higher in the BNCT group. This result can be explained by the fact that DSBs induced by high LET radiation are densely concentrated in clusters (Bracalante et al. 2013) and the large focus size reflects high DSB complexity (Staaf et al. 2012). After 24 h we observed that focus frequencies tended to decrease in all treatment groups. However, the focus size remained constant, indicating that repair processes have been activated but that only small foci disappear. Large foci are persistent and difficult to repair (Staaf et al. 2012).

Two different pathways that mediate DSB repair have been identified in mammalian cells: HRR and NHEJ. The HRR pathway is a very accurate repair mechanism, in which homologous DNA on a sister chromatid or chromosome works as a template to guide repair of the broken strand. NHEJ, on the other hand, is a less accurate form of DSB repair, in which the two ends of the broken DNA molecule are processed to form compatible edges that are directly ligated. It is not completely clear what exactly determines the activation of HRR or NHEJ, but the cell cycle stage is thought to play an important role in this decision (Jeggo and Lobrich 2006). A number of repair proteins appear to be regulated by checkpoints genes or to be the substrates for checkpoint kinases (Pawlik and Keyomarsi 2004). When we analyzed repair pathways induced by BNCT in follicular carcinoma cells compared to the non-irradiated and gamma irradiated cells, we observed an increase of Rad51 and Rad54 mRNA expression at 4 and 6 h after the irradiation, respectively, showing the expression of enzymes belonging to the HRR pathway. We also studied protein expression by Western blot and observed an increase of Rad51 protein 4 h after the irradiation and that it remained elevated for 48 h. This is consistent with an increased transcription followed by the translation process. The expression of Ku70, a member of NHEJ, did not show significant changes with respect to the basal levels. The results demonstrated that in the follicular thyroid carcinoma cell line, the main activated repair pathway is HRR. This is consistent with our previous study, where WRO cells were arrested after BNCT irradiation in the G_2 phase (Perona et al. 2013). HRR provides highly accurate DSB repair by using an intact sister chromatid as template and it is therefore restricted to the late S and G_2 phase (Sonoda et al. 2006).

To find out if the damage profile and the repair pathways induced by BNCT in WRO cell line were tissue specific, we performed the same analysis in a melanoma cell line (Mel J). Mel J is a highly heterogeneous human melanoma cell line, which contains small cells, dendritic cells and mega cells with multiple nuclei (Guerra et al. 1990). We observed that the γH2AX focus pattern over time is different to that seen in thyroid carcinoma cells. The highest number of γH2AX foci were detected 30 min after irradiation in the N and BNCT groups showing a slight decrease at 24 h. The largest foci were observed in the BNCT group 30 min after radiation exposure, and they seemed to reach the basal level at 24 h. These results could suggest that in the melanoma cell line, the lower biological effectiveness observed compared to the thyroid cell line could be related to the fact that DSBs are more scattered and better distributed along the DNA molecule, resulting in a more efficient DNA repair process (Belli et al. 2002). The repair pathway analysis showed that both HRR and NHEJ were induced in melanoma cells by the radiation arising from BNCT. We demonstrated an increase in Rad51 mRNA after 2 h and a marked increase in the Ku70 mRNA at 4 h. NHEJ is the predominant pathway for DSB repair in mammalian species and it can function independently of the cell cycle phase (Jeggo and Lobrich 2006). The pathway selection can be a simple competition between HRR and NHEJ (Yano et al. 2009). Another postulated mechanism for pathway selection is the recruitment of the Ku protein to the site of a DSB. This hypothesis is based in the fact that Ku is abundant in the nucleus throughout the cell cycle and it has an extremely high affinity to DNA ends (Yano et al. 2009). Interestingly, Kim et al. reported that Ku is actually recruited to DSBs prior to Rad51, the central protein in HRR (Kim et al. 2005).

Thyroid cancer can be found in a differentiated or undifferentiated form. Differentiated forms, like papillary or follicular carcinomas, have a generally good prognosis. Most of them, but not all, present a normal iodine uptake and, therefore, successful surgical thyroidectomy can be achieved with a ^{131}I therapeutic dose. In many cases, these types are well

controlled and complete remission of the tumor is obtained. In other instances, the prognosis is not so good. The undifferentiated thyroid carcinoma or the recurrences of some differentiated forms lost their capability to concentrate iodine, and therefore, the therapeutic effect of the radioactive iodine is missing (Chiacchio et al. 2008). As a consequence, new treatments are being explored to offer new alternatives to patients in these cancer stages. Some years ago, we started to study the possibility of applying BNCT for the treatment of such cases. We evaluated different strategies to optimize the performance of BNCT and to obtain better results. The studies performed here showed that thyroid carcinoma had a particular pattern of DNA DBS damage and the mechanisms of repair induced are different from those in melanoma cells. This understanding will allow us to evaluate different blocking points, to potentiate the damage to tumor cells. A future strategy to manipulate the thyroid cancer response to BNCT would be to administer an inhibitor of Rad51.

Acknowledgements A part of these studies was supported by grants from the Scientific and Technical Research National Council (CONICET) and Secretary of Science and Technology (SEPCYT).

Compliance with ethical standards

Conflict of interest We declare that there is no conflict of interest in this paper.

References

Aihara T, Hiratsuka J, Morita N, Uno M, Sakurai Y, Maruhashi A, Ono K, Harada T (2006) First clinical case of boron neutron capture therapy for head and neck malignancies using ^{18}F-BPA PET. Head Neck 28(9):850–855

Aiyama H, Nakai K, Yamamoto T, Nariai T, Kumada H, Ishikawa E, Isobe T, Endo K, Takada T, Yoshida F, Shibata Y, Matsumura A (2011) A clinical trial protocol for second line treatment of malignant brain tumors with BNCT at University of Tsukuba. Appl Radiat Isot 69(12):1819–1822

Antonelli F, Campa A, Esposito G, Giardullo P, Belli M, Dini V, Meschini S, Simone G, Sorrentino E, Gerardi S, Cirrone GA, Tabocchini MA. (2015). Induction and Repair of DNA DSB as Revealed by H2AX Phosphorylation Foci in Human Fibroblasts Exposed to Low- and High-LET radiation: relationship with early and delayed reproductive cell death. Radiat Res 183(4):417–431. https://doi.org/10.1667/RR13855.1

Belli M, Sapora O, Tabocchini MA (2002) Molecular targets in cellular response to ionizing radiation and implications in space radiation protection. J Radiat Res 43:13–19

Bracalente C, Ibañez I, Molinari B, Palmieri M, Kreiner A, Valda A, Davidson J, Durán H (2013). Induction and persistence of large γH2AX foci by high linear energy transfer radiation in DNA-dependent protein kinase-deficient cells. Int J Radiat Oncol Biol Phys 87(4):785–794

Burma S, Chen BP, Murphy M, Kurimasa A, Chen DJ (2001) ATM phosphorylates histone H2AX in response to DNA double-strand breaks. J Biol Chem 276(45):42462–42467

Busse PM, Harling OK, Palmer MR, Kiger WS 3rd, Kaplan J, Kaplan I, Chuang CF, Goorley JT, Riley KJ, Newton TH, Santa Cruz GA, Lu XQ, Zamenhof RG (2003) A critical examination of the results from the Harvard-MIT NCT program phase I clinical trial of neutron capture therapy for intracranial disease. J Neurooncol 62(1–2):111–121

Chiacchio S, Lorenzoni A, Boni G, Rubello D, Elisei R, Mariani G (2008) Anaplastic thyroid cancer: prevalence, diagnosis and treatment. Minerva Endocrinol 33(4):341–357

Coderre JA, Morris GM (1999) The radiation biology of Boron Neutron Capture Therapy. Radiat Res 151(1):1–18

Dagrosa MA, Viaggi M, Kreimann E, Farías S, Garavaglia R, Agote M, Cabrini RL, Dadino JL, Juvenal GJ, Pisarev MA (2002) Selective uptake of p-borophenylalanine by undifferentiated thyroid carcinoma for boron neutron capture therapy. Thyroid 12(1):7–12

Dagrosa MA, Viaggi M, Longhino J, Calzetta O, Cabrini R, Edreira M, Juvenal G, Pisarev MA (2003) Experimental application of boron neutron capture therapy to undifferentiated thyroid carcinoma. Int J Radiat Oncol Biol Phys 57(4):1084–1092

Dagrosa MA, Thomasz L, Longhino J, Perona M, Calzetta O, Blaumann H, Rebagliati RJ, Cabrini R, Kahl S, Juvenal GJ, Pisarev MA (2007) Optimization of boron neutron capture therapy for the treatment of undifferentiated thyroid cancer. Int J Radiat Oncol Biol Phys 69(4):1059–1066

Dagrosa A, Carpano M, Perona M, Thomasz L, Nievas S, Cabrini R, Juvenal G, Pisarev M (2011a) Studies for the application of boron neutron capture therapy to the treatment of differentiated thyroid cancer. Appl Radiat Isot 69(12):1752–1755

Dagrosa MA, Crivello M, Perona M, Thorp S, Santa Cruz GA, Pozzi E, Casal M, Thomasz L, Cabrini R, Kahl S, Juvenal GJ, Pisarev MA (2011b) First evaluation of the biologic effectiveness factors of boron neutron capture therapy (BNCT) in a human colon carcinoma cell line. Int J Radiat Oncol Biol Phys 79(1):262–268

Dudás A, Chovanec M (2004) DNA double-strand break repair by homologous recombination. Mutat Res 566(2):131–167

Guerra L, Bover L, Mordoh J (1990) Differentiating effect of L-tyrosine on the human melanoma cells line IIB-MEL. Exp Cell Res 188(1):61–65

Ibañez I, Bracalante C, Molinari B, Palmieri M, Policastro L, Kreiner A, Burlon A, Valda A, Navalesi D, Davidson J, Davidson M, Vazquez M, Ozafrán M, Durán H (2009). Induction and rejoining of DNA double strand breaks assessed by H2AX phosphorylation in melanoma cells irradiated with proton and lithium beams. Int J Radiat Oncol Biol Phys, 74(4):1226–1235

Jeggo P, Löbrich M (2006) Radiation-induced DNA damage responses. Radiat Prot Dosimetry 122(1–4):124–127

Jen-Chung Ko Shih-CiCiou, Cheng C-M, Wang L-H, Hong J-H, Jheng M-Y, Ling S, Lin Y (2008) Involvement of Rad51 in cytotoxicity induced by epidermal growth factor receptor inhibitor (gefitinib, IressaR) and chemotherapeutic agents in human lung cancer cells. Carcinogenesis 29(7):1448–1458

Joensuu H, Kankaanranta L, Tenhunen M, Saarilahti K (2011) Boron Neutron Capture Therapy (BNCT) as cancer treatment. Duodecim 127(16):1697–1703

Kim JS, Krasieva TB, Kurumizaka H, Chen DJ, Taylor AM, Yokomori K (2005) Independent and sequential recruitment of NHEJ and HR factors to DNA damage sites in mammalian cells. J Cell Biol 170(3):341–347

Korabiowska M, Quentin T, Schlott T, Bauer H, Kunze E (2004) Down-regulation of Ku 70 Ku 80 mRNA expression in transitional cell carcinomas of the urinary bladder related to tumor progression. World J Urol 2(6):431–440

Lieber MR (2010) The mechanism of double-strand DNA break repair by the non homologous DNA end-joining pathway. Annu Rev Biochem 79:181–211

Maier P, Hartmann L, Wenz F, Herskind C (2016) Cellular pathways in response to ionizing radiation and their targetability for tumor radiosensitization. Int J Mol Sci. https://doi.org/10.3390/ijms17010102

Matsuda M, Miyagawa K, Takahashi M, Fukuda T, Kataoka T, Asahara T, Inui H, Watatani M, Yasutomi M, Kamada N, Dohi K, Kamiya K (1999) Mutations in the RAD54 recombination gene in primary cancers. Oncogene 18:3427–3430

Miller M, Quintana J, Ojeda J, Langan S, Thorp S, Pozzi E, Sztejnberg M, Estryk G, Nosal R, Saire E, Agrazar H, Graiño F (2009) New irradiation facility for biomedical applications at the RA-3 reactor thermal column. Appl Radiat Isot 67(7–8 Suppl):S226-9

Olive PL (1998) The role of DNA single- and double-strand breaks in cell killing by ionizing radiation. Radiat Res 150(5 Suppl):S42–S51

Pasieka JL (2003) Anaplastic thyroid cancer. Curr Opin Oncol 15(1):78–83

Pawlik TM, Keyomarsi K (2004) Role of cell cycle in mediating sensitivity to radiotherapy. Int J Radiat Oncol Biol Phys 59(4):928–942

Perona M, Rodríguez C, Carpano M, Thomasz L, Nievas S, Olivera M, Thorp S, Curotto P, Pozzi E, Kahl S, Pisarev M, Juvenal G, Dagrosa A (2013). Improvement of the Boron Neutron Capture therapy (BNCT) by the previous administration of the histone deacetylase inhibitor sodium butyrate for the treatment of thyroid carcinoma. Radiat Environ Biophys. 52(3):363–373

Redon CE, Nakamura AJ, Zhang YW (2010) Histone gamma H2AX and poly (ADP-ribose) as clinical pharmacodynamics biomarkers. Clin Cancer Res, 16:4532–4542

Sigurdsson S, Van Komen S, Petukhova G, Sung P (2002) Homologous DNA pairing by human recombination factors Rad51 and Rad54. J Biol Chem 277(45):42790–42794

Sonoda E, Hochegger H, Saberi A, Taniguchi Y, Takeda S (2006) Differential usage of non-homologous end joining and homologous recombination in double strand break repair. DNA Rep 5:1021–1029

Staaf E, Brehwens K, Haghdoost S, Czub J, Wojcik A (2012) Gamma-H2AX foci in cells exposed to a mixed beam of X-rays and alpha particles. Genome Integrity 3(1):8. https://doi.org/10.1186/2041-9414-3-8

Vermeulen C, Verwijs-Janssen M, Begg AC, Vens C (2008) Cell cycle phase dependent role of DNA polymerase beta in DNA repair and survival after ionizing radiation. Radiother Oncol 86(3):391–398

Wang H, Zhang X, Wang P, Yu X, Essers J, Chen D, Kanaar R, Takeda S, Wang Y (2010) Characteristics of DNA-binding proteins determine the biological sensitivity to high-linear energy transfer radiation. Nucleic Acids Res 38(10):3245–3251

Weterings E, Chen DJ (2008) The endless tale of non-homologous end-joining. Cell Res 18:114–124

Yano K, Morotomi-Yano K, Adachi N, Akiyama H (2009) Molecular mechanism of protein assembly on DNA double-strand breaks in the non-homologous end-joining pathway. J Radiat Res 50(2):97–108